Journal of Molecular Catalysis A: Chemical 353–354 (2012) 1–6

Contents lists available at SciVerse ScienceDirect

Journal of Molecular Catalysis A: Chemical

journal homepage: www.elsevier.com/locate/molcata

Editor's Choice paper

A computational comparison of Ni^{II} and Pt^{II} hydrido-tris(pyrazolyl)borate supported hydroarylation catalysis

Thomas R. Cundari*, Hector E. Gonzalez

Department of Chemistry for Advanced Scientific Computing and Modeling (CASCaM), University of North Texas, P.O. Box 305070, Denton, TX 76203-5070, United States

ARTICLE INFO

Article history:
Received 19 October 2011
Accepted 1 November 2011
Available online 7 November 2011

Keywords:
TpPtII
TpNiII
Olefin hydroarylation

ABSTRACT

As alkyl-arenes are important feedstock chemicals, synthetic methods more atom economical than traditional Friedel-Crafts and bond-coupling reactions are needed. Pt^{II} complexes have been experimentally demonstrated to facilitate olefin hydroarylation. A $TpPt^{II}$ catalyst model (Tp = hydrido-*tris*(pyrazolyl)borate) was selected for computational studies. Nickel's low cost prompted its evaluation as it is isoelectronic to platinum. Computational results indicate that nickel and platinum operate through different mechanisms. The TpPt catalyst model activates benzene through a two-step oxidative addition/reductive elimination mechanism with a Pt^{IV} intermediate. However, the TpNi catalyst forms ethylbenzene product and closes the catalytic loop via a single step (sigma-bond metathesis) mechanism. Despite these differences in mechanism, comparable energy barriers (differing by *ca.* 2 kcal/mol), are derived from density functional theory (DFT) simulations. The present results suggest that attempts to "reverse engineer" precious metal catalyst substitutes with Earth-abundant metals (*e.g.*, Pt → Ni) may require reconsideration of typical structure–property relationships in catalyst design.

1. Introduction

As the goal of sustainability becomes more urgent, chemists are motivated to seek approaches that maximize atom economy. The industrial importance and scale at which they are produced designates alkyl-arenes (ArR) as lucrative targets for improved manufacturing techniques, both in terms of waste reduction as well as resource consumption, *e.g.*, direct functionalization of benzene as opposed to multi-step Friedel-Crafts chemistry via aryl-halides. This note focuses on the catalytic formation of ethylbenzene from ethylene and benzene. Widespread efforts have been undertaken by numerous groups to expand established coupling and insertion reactions with σ-bond metathesis and related reactions to form complete catalytic cycles. For example, research by the Cundari and Gunnoe groups focused on octahedral d^6 Ru catalysts for olefin hydroarylation. The impact of ligand steric and electronic profile on the thermodynamics and kinetics of main cycle and side reactions was analyzed [1]. A square planar Pt^{II} catalyst was recently reported by Gunnoe and coworkers using ^{t}bpy (4,4′-di-*tert*-butyl-2,2′-bipyridine) as the ancillary ligand. In some respects, the latter proved too active, in that it suffered from facilitating double alkylation, thus leading to dialkyl-arenes (ArR_2) [2]. Tilley and coworkers have also probed hydroarylation via Pt^{II} complexes [3–5]. Periana and Goddard et al. have investigated the use of Ir-based catalysts in particular those with acetylacetonate supporting ligands for hydroarylation catalysis [6–8].

A preliminary computational study of $[bpyPt(Ph)]^+$-catalyzed hydroarylation implied that bulky supporting ligands should be considered [9]. Hydrido-*tris*(pyrazolyl)borate, Tp, was selected for this research given its use as a supporting ligand in Ru^{II}-catalyzed hydroarylation [1]. Like bpy, Tp coordinates via a lone pair on N. Templeton and Goldberg have studied $TpPt^{II/IV}$ complexes, which exploit Tp's ability to possess either κ^2 or κ^3 coordination, and which effect reductive elimination and oxidative addition pathways [10], reactions integral to olefin hydroarylation catalysis.

In this study, the main focus is the formation of C_{sp2}–C_{sp3} bonds in the main catalytic cycle (the issue of side reactions is ignored). Analysis of Ni in this study was deemed potentially advantageous as it and Pt possess d^8 electronic configurations for the 2+ formal oxidation state, while Ni is more abundant and much cheaper than Pt [11–13]. Moreover, research has been reported on the ability of nickel complexes to form C–C bonds and activate C–H bonds [14,15]. Finally, scorpionate-supported Ni complexes have been synthesized as models for metalloenzyme studies [16]. The cationic nature of $[bpyPt(Ph)]^+$ catalysts was suggested to contribute to the formation of ArR_2 side-products in preliminary modeling [2,17,18], further motivating the use of an anionic supporting ligands such as Tp, and hence an overall neutral Group 10 catalyst. Finally, it is anticipated that the modeling results presented here could motivate further study of nickel catalysts for bond coupling catalysis

* Corresponding author.
E-mail address: t@unt.edu (T.R. Cundari).

1381-1169/$ – see front matter © 2011 Elsevier B.V. All rights reserved.
doi:10.1016/j.molcata.2011.11.007

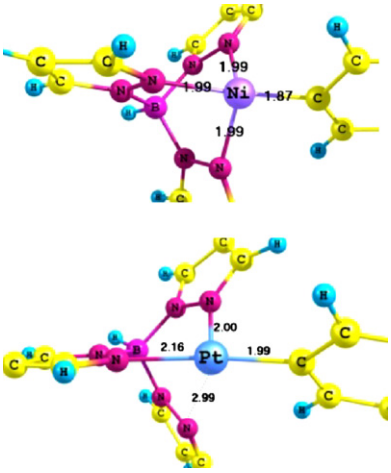

Fig. 1. Core geometries of [κ^3-TpNi(Ph)] and [κ^2-TpPt(Ph)] catalyst models. Calculated bond lengths in Å.

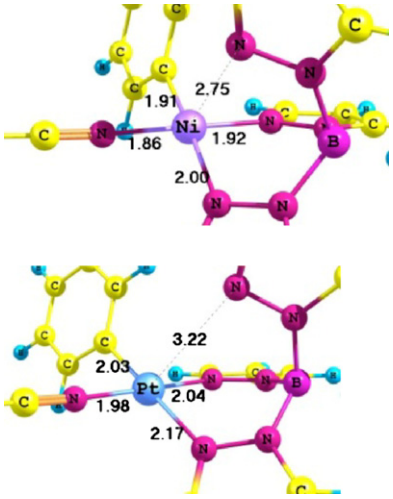

Fig. 2. Core geometries of [κ^2-TpNi(Ph)(NCMe)] and [κ^2-TpPt(Ph)(NCMe)], catalyst precursor. Calculated bond lengths in Å.

given the current interest in the greater use of Earth abundant metal catalysts.

2. Computational methods

All calculations were performed with the Gaussian 03 [19] software package. The systems were treated with the Stevens valence basis sets/pseudopotentials, CEP-31G [20–23], in conjunction with the B3LYP [24–26] functional. Polarization basis functions were added to the main group elements using exponents taken from the 6-31G(d) all-electron basis sets. The criterion for transition states (TS) was that of only one imaginary frequency, marking them as local maxima, through the calculation of the energy Hessian. All other stationary points had no imaginary frequencies, indicating them to be local minima. Gibbs free energies were calculated at 298.15 K and 1 atm using unscaled vibrational frequencies.

3. Results and discussion

3.1. Stationary point geometries

Computed stationary point geometries for Ni^{II} and Pt^{II} models are consistent with previous DFT studies [1,14] and experiment [10]. Optimized geometries of related Ni^{II} and Pt^{II} complexes showed great similarity, with the main differences being bond length changes of ~0.1 Å in the form of shorter Ni–N,C bonds, as expected. The remainder of this section focuses on stationary points for which there are disparities between Ni^{II} and Pt^{II} geometries, as these may be expected to manifest differences in calculated energetics (*vide infra*) for the olefin hydroarylation catalytic cycle.

Calculations of the hydroarylation catalytic cycle were carried out on both TpPt and TpNi models, starting with active species with a potentially open coordination site (*i.e.*, TpMPh (M = Ni, Pt)) for subsequent ethylene coordination. The TpNiPh complex had a distorted T_d geometry as suggested by the symmetrical Ni–N bond lengths (NiN ~ 1.99 Å), (Fig. 1) (left), while the Pt congener had a square planar (SQ_4) geometry, (Fig. 1) (right). The Pt–N bond trans to the open coordination site is shorter (2.00 Å) than that *trans* to the phenyl ligand (2.16 Å) These results for optimized TpMPh geometries coincide with simple expectations from crystal field theory given the smaller d-orbital splitting for Ni^{II} *vs.* Pt^{II} and then greater propensity for the latter metal to assume a SQ_4 geometry in its divalent state. {A search of the Cambridge Structural Database supports that NiL_4 complexes are as likely to adopt a SQ_4 geometry as they are to adopt a T_d one. PtL_4 complexes on the other hand overwhelmingly prefer SQ_4 geometries [27]}. Interestingly, the Tp supporting ligand is κ^3 for the nickel catalyst model, but κ^2 for the platinum complex. For the latter, the Pt–N distance for the non-coordinated Tp pyrazolate arm is calculated to be 2.99 Å.

The 16-electron catalyst precursors, TpMPh(NCMe), which has a coordinated acetonitrile, makes the Ni^{II} system square planar just like the Pt^{II}, (Fig. 2). A square planar description is now apt for TpPtPh(NCMe) given the elongated Pt–N distance of 3.22 Å for the third Tp arm *vs.* ~2.08 Å for the other two pyrazolate arms, (Fig. 2) (right). One arm of Tp is consistently longer than the other two bonds for both the modeled Pt and Ni complexes leading us to label TpMPh(NCMe) as having a κ^2 coordination mode; in the case of platinum the prediction of κ^2-Tp coordination is consistent with experimental structures [10]. Additionally, the data imply there is reasonably facile κ^2/κ^3 equilibrium in these Group 10 Tp complexes, which could be advantageous vis-à-vis catalysis.

Ethylene coordination, (Fig. 3), to TpMPh followed by olefin (C=C) insertion into the metal–phenyl bond, leads to the formation of a phenethyl ligand and the C_{sp2}–C_{sp3} bond of interest. In Table 1, selected bond lengths and angles are presented that demonstrate the good accord between our calculated results, [TpPt(Ph)(C_2H_4)], (Fig. 3) (left), and experiment [10].

The transition state for ethylene insertion into the metal–phenyl bond shows the elongation of the C–C bond *vs.* that in the ethylene adduct precursor, and pyramidalization of the ethylene hydrogens as the two carbon atoms they are bonded to transition from sp^2 to sp^3 hybridization, (Fig. 4). The next step in the catalytic cycle after formation of the CH_2CH_2Ph ligand is the coordination of benzene to [κ^2-TpM(C_2H_4Ph)], M = Ni, Pt. Note that upon benzene binding, the two Group 10 metals, which are similar to this point, diverge in mechanism for C–H bond activation and product (ethylbenzene) release, a point that we will return to below.

The binding of benzene to κ^2-TpPt(CH_2CH_2Ph) allows for a saturated, 16-electron, square planar coordination sphere for κ^2-TpPt(CH_2CH_2Ph)(η^2-C_6H_6). However, for the Ni congener, Ni–C distances to the benzene "ligand" are very large, ~3.44 Å. Indeed, Ni is more stabilized by the Tp ligand that, like in the TpNiPh catalyst discussed above, has reverted from κ^2 to κ^3 coordination, (Fig. 5), *i.e.*, κ^3-TpPt(CH_2CH_2Ph)·C_6H_6.

The calculated transition state and intermediate geometries indicate that C–H bond activation to form PhEt and close the catalytic cycle represents the most significant divergence between the Pt^{II} and Ni^{II} model catalysts. The TpPt catalyst model activates benzene through a two-step oxidative addition/reductive elimination

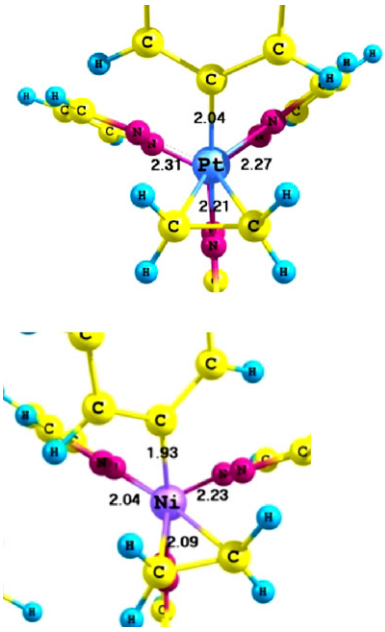

Fig. 3. Core geometries of [TpPt(Ph)(C_2H_4)] and [TpNi(Ph)(C_2H_4)]. Calculated bond lengths in Å. Pt–C distances to C_2H_4 ligand = 2.11 Å; Ni–C for C_2H_4 ligand = 2.03 and 2.07 Å.

Table 1
Comparison of corresponding bond lengths and angles of [TpPt(Ph)(C_2H_4)], (Fig. 3) (left), with experimental results [10].

	Calculated	Experimental
Pt–C (benzene)	2.040 Å	2.104 Å
Pt–C (ethylene)	2.108–2.114 Å	2.064–2.052 Å
C–C (ethylene)	1.458 Å	1.43 Å
Pt–N (Tp)	2.212–2.313 Å	2.140–2.220 Å
C (Et)–Pt–C (Et)	40.4°	40.2°
C (Bz)–Pt–C (Et)	88.3–88.8°	90.4–92.0°

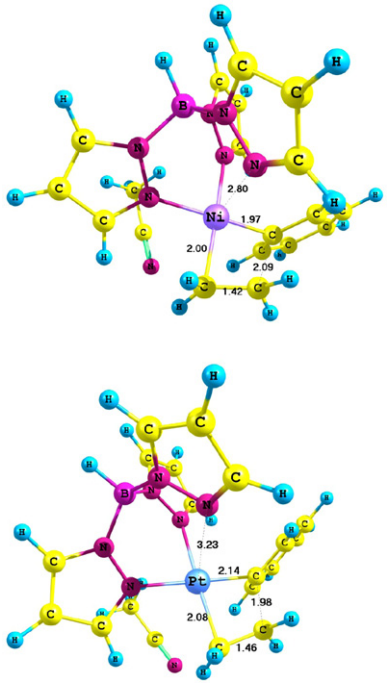

Fig. 4. Core geometries of [TpPt(Ph)(C_2H_4)]‡ and [TpNi(Ph)(C_2H_4)]‡ ethylene insertion for phenethyl formation. Calculated bond lengths in Å.

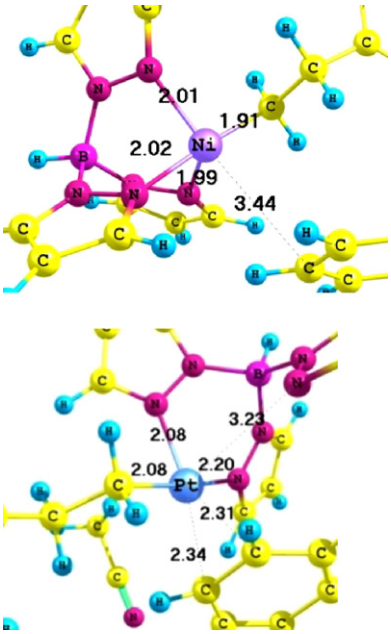

Fig. 5. Core geometries of [TpNi(C_6H_6)(C_2H_4Ph)] (left), a tetrahedral Ni complex with benzene in the outer coordination sphere, and [κ^2-TpPt(C_2H_4Ph)(C_6H_6)] (right) a square planar Pt complex with benzene in the inner coordination sphere. Calculated bond lengths in Å.

mechanism with a Pt^{IV} intermediate. {No sigma-bond metathesis TS could be isolated despite numerous attempts to isolate such a stationary point.} However, the TpNi catalyst operates via a single step (sigma-bond metathesis TS) to form ethylbenzene product and close the catalytic loop. {An oxidative addition TS could not be found.} The present results are consistent with a recent DFT study of C–H activation by bpyM (M = Group 10 metal) reported by Butschke and co-workers [14]. In their study Butschke found that Ni operated via a single-step mechanism while Pt activated C–H bonds via a two-step pathway.

As noted above, there is a sizeable difference in the mechanisms for TpPt and TpNi C–H bond activation to close the catalytic loop. The Ni system is thus calculated to proceed via a one-step, sigma-bond metathesis type mechanism, (Fig. 6), with the Pt catalyst model operating, (Figs. 7 and 8), via a two-step, oxidative addition/reductive elimination pathway to release ethylbenzene. Calculations predict that the Pt^{IV}-hydride intermediate is an octahedral complex, as expected for a d^6, six-coordinate complex. Presumably, these differences in C–H activation mechanisms for nickel *vs.* platinum reflect the greater stability of the 4+ formal oxidation state of the heavier metal platinum.

The single-step benzene C–H activation mechanism for the $TpNi^{II}$ system is analogous to previously studied $TpRu^{II}$ systems. The $TpPt^{IV}$–H intermediate suggests a possible side reaction from transfer of the hydride to the free arm of Tp, (Fig. 8), which has been seen experimentally by Templeton et al. [28]. DFT calculations indicate that the Pt-hydride is more stable than the protonated-Tp

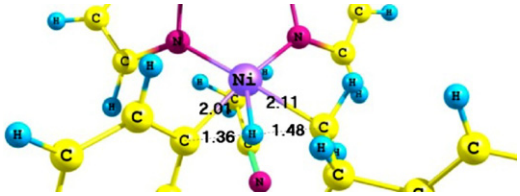

Fig. 6. Core geometry of [κ^2-TpNi(Ph)(H)(C_2H_4Ph)]‡, the sigma-bond metathesis transition state. Calculated bond lengths in Å.

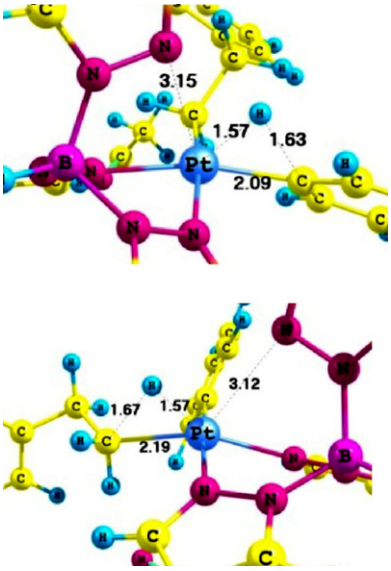

Fig. 7. Core geometries of transition states for benzene C–H oxidative addition (left) and ethylbenzene C–H reductive elimination (right). Calculated bond lengths in Å.

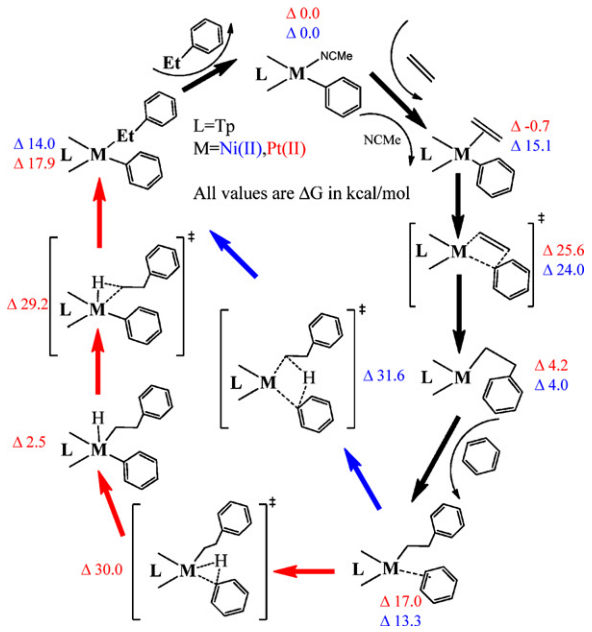

Scheme 1. Catalytic cycle for ethylene hydrophenylation with calculated free energies (in kcal/mol) relative to the TpMPhNCMe catalyst precursor for nickel (blue) and platinum (red). (For interpretation of the references to color in this figure legend, the reader is referred to the web version of the article.)

isomer, (Fig. 8), by only 5.4 kcal/mol, consistent with its observation by Templeton et al. {Note that we were unable to find a transition state that connects these two tautomers.}

4. Calculated energetics

The differences in stationary point geometry immediately suggest potentially interesting differences in the calculated kinetics and thermodynamics for the TpMPh-catalyzed ethylene hydrophenylation. However, in many cases, the energetic differences (Scheme 1) are negligible! For example, the calculated free energy barriers for olefin insertion differ by <2 kcal/mol (24.0 kcal/mol for TpNi catalysts and 25.6 for the TpPt catalyst model) with the TpNi having the lower insertion barrier, (Scheme 1). On the other hand, despite the differences in the predicted pathways to C–H activation of benzene to close the catalytic loop, Pt^{II} has only slightly lower barriers for hydrogen transfer to form the PhEt product. For the two-step, Pt^{IV}-mediated processes, the initial oxidative addition of benzene has a calculated barrier of 30.0 kcal/mol while the reductive elimination to form PhEt is slightly lower at 29.2 kcal/mol, (Scheme 1), as compared to the single hydrogen transfer barrier of the Ni^{II} catalyst of 31.6 kcal/mol. Based on earlier modeling of hydroarylation catalysis [1,9,29], these results imply that one might expect that TpNi and TpPt catalysts to have similar activity and turnover frequency.

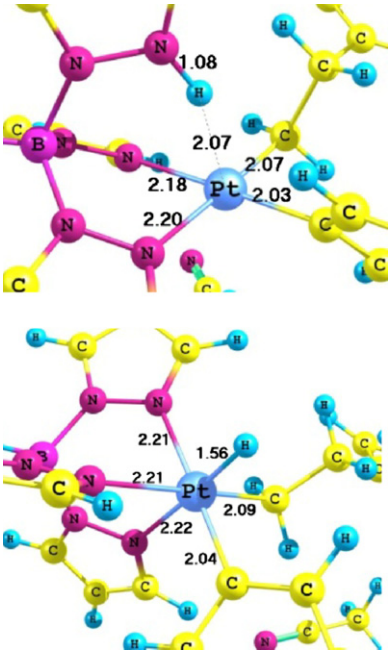

Fig. 8. Core geometries of [κ^2-HTpPt(Ph)(C_2H_4Ph)], a side reaction product (previously observed experimentally) [28] and [TpPt(H)(Ph)(C_2H_4Ph)], the Pt^{IV}-hydride intermediate. Calculated bond lengths in Å.

In a case where the geometries for the Ni^{II} and Pt^{II} complexes show only a minor variation (see Fig. 3), the ethylene adducts show significant energetic differences. Specifically, binding of ethylene to produce κ^2-TpPt(Ph)(C_2H_4) stabilizes the Pt^{II} complex Tp(Ph)Pt by 25.7 kcal/mol but destabilizes the Ni^{II} by 4.1 kcal/mol. The mildly endergonic binding of ethylene to the TpNi catalyst is a reflection of the weak binding enthalpy being countermanded by the unfavorable $T\Delta S$ contribution to ligand binding.

Analyzing calculated geometries more closely (see Fig. 5) reveals more differences in binding of benzene as a function of metal than is suggested by the calculated energetics. To wit, the κ^3-TpNi(CH_2CH_2Ph)·C_6H_6 complex is only 3.7 kcal/mol more stable in relation to the catalyst ground state than is κ^2-TpPt(CH_2CH_2Ph)(C_6H_6), ΔG_{rel} = 17.0 kcal/mol, (Scheme 1). Presumably, the small relative free energy difference is a result of the Tp complex in the former Ni complex having κ^3 and not κ^2 coordination, which more than compensates for the missing π donation from benzene to the metal center in the latter Pt complex.

As discussed by Morello and coworkers in their study of hydroarylation by Group 8 TpM complexes [29], the 3d metals with their smaller ionic radii sometimes preferentially coordinate weakly binding ligands like benzene in the outer sphere when they have scorpionate supporting ligation. This dichotomy is reflected in "movement" of the Tp ligand between κ^2 and κ^3 coordination modes. This change in hapticity within a transition metal triad has been seen before as has the ease of inter-conversion [30,31].

While one may assume an important role for this κ^3/κ^2 equilibrium in catalysis, the present modeling results are interesting in that they indicate that large changes in coordination geometry do not impart large changes in catalytic cycle energetics. However, one may deduce from the present and past modeling results [1,29], that the inability to form weakly bound benzene precursors prior to their C–H activation, while it may not impact the effective barriers, may retard catalyst activity through the pre-exponential factor in the Arrhenius equation.

While the mechanism (sigma-bond metathesis *vs.* oxidative addition/reductive elimination) and the binding modes (inner *vs.* outer sphere benzene and κ^2/κ^3 equilibrium) for Ni and Pt can vary significantly, the TS energetics including that for the calculated rate determining step of the catalytic cycle does not. The ethylene insertion TS, (Fig. 4), has only 1 kcal/mol relative free energy difference between both metals (see Scheme 1). For the C–H activation transition states, the Pt models are lower than the Ni congeners by ~2 kcal/mol. {We note that the present results are consistent with previous studies that also showed C–H activation as the rate determining step [1].} The present DFT results also suggest that Ni is a strong candidate for hydroarylation catalysis for large industrial process, although further work on possible side reactions is required.

5. Summary and conclusions

While bpyPt-based hydroarylation catalysts suffered from a second alkylation [2], its lack of other side reactions (*e.g.*, vinylic C–H activation) made it a viable candidate for further catalyst tuning, thus partially motivating the present research. C–H bond activation barriers were in the same range for both bpy [9] and hydrido-*tris*(pyrazolyl)borate (present work) supporting ligands [9]. The C=C insertion barrier into the metal–phenyl bond is, on the other hand, ~15 kcal/mol less for bpyPt than for TpPt catalysts, an indication that perhaps an electrophilic, cationic system is important for facile C=C insertion. At this time further work into Ni hydroarylation catalysts, experimental and computational, seems warranted, but the problem of coordination sphere crowding (see Fig. 5) in Tp complexes of 3d metals still needs attention. The model TpPtPh is suggested from computations to operate via an oxidative addition/reductive elimination pathway akin to that for bpyPt [9]; as in that case, these two-step, Pt^{IV}-mediated catalytic cycles are close in energy to sigma-bond metathesis pathways.

Results for TpNi and TpPt catalysts are comparable, but do not offer exceptional improvement upon a previous study on octahedral, Group 8 complexes supported by scorpionate ligands: the calculated ethylene insertion barriers energy range from 4.3 to 16.2 kcal/mol and benzene C–H bond activation ~20.1–30.8 kcal/mol, depending primarily on the central metal ion (Ru^{II} *vs.* Os^{II}) [29]. Given a choice between the two catalysts modeled herein, $TpNi^{II}$ has an advantage over $TpPt^{II}$ because the latter goes through a two-step benzene C–H bond activation pathway. Our calculations demonstrate a possible side reaction, the addition of hydrogen to the free arm of Tp, which may thus impede hydroarylation catalysis for Pt^{II}-scorpionate catalysts. That is, however, not to say that Ni^{II}-scorpionate catalysts are ideal as the expected difficulties brought about by coordination of weakly bound ligands within the catalytic cycle, due to the smaller size of 3d metals, still need to be overcome.

While the prevailing norm in catalyst modeling is that small changes in geometry portend larger changes in energetics, the present case is a rare example that contradicts this common structure–property assumption in catalyst design. One might speculate that this is due to the considerable differences in light and heavy transition metal–ligand bonding, vis-à-vis the covalency/ionicity of metal–ligand bonds, ligand field splitting or what Wolczanski has termed the "density of states" model [32]. Alterations in expected catalyst structure–property relationships signals an important challenge given the current motivation to reverse engineer successful precious metal (typically 4d and 5d metals) catalysts with more Earth-abundant (typically 3d) base metal replacements.

Acknowledgements

The authors acknowledge the NSF for facility support (CHE-0741936) and US Department of Energy, Office of Basic Energy Sciences, Catalysis Science Program for their support of this research (DE-FG02-03ER15387).

Appendix A. Supplementary data

Supplementary data associated with this article can be found, in the online version, at doi:10.1016/j.molcata.2011.11.007.

References

[1] N.A. Foley, J.P. Lee, Z. Ke, T.B. Gunnoe, T.R. Cundari, Acc. Chem. Res. 42 (2009) 585–597.
[2] B.A. McKeown, N.A. Foley, J.P. Lee, T.B. Gunnoe, Organometallics 27 (2008) 4031–4033.
[3] D. Karshtedt, J.L. McBee, A.T. Bell, T.D. Tilley, Organometallics 25 (2006) 1801–1811.
[4] J.L. McBee, A.T. Bell, T.D. Tilley, J. Am. Chem. Soc. 130 (2008) 16562–16571.
[5] J.L. McBee, T.D. Tilley, Organometallics 29 (2009) 184–192.
[6] G. Bhalla, J. Oxgaard, W.A. Goddard, R.A. Periana, Organometallics 24 (2005) 3229–3232.
[7] S.M. Bischof, D.H. Ess, S.K. Meier, J. Oxgaard, R.J. Nielsen, G. Bhalla, W.A. Goddard, R.A. Periana, Organometallics 29 (2010) 742–756.
[8] J. Oxgaard, R.A. Periana, W.A. Goddard, J. Am. Chem. Soc. 126 (2004) 11658–11665.
[9] B.A. McKeown, H. Gonzalez, M. Friedfeld, T.B. Gunnoe, T.R. Cundari, M. Sabat, J. Am. Chem. Soc. 133 (2011) 19131–19152.
[10] M.P. Jensen, D.D. Wick, S. Reinartz, P.S. White, J.L. Templeton, K.I. Goldberg, J. Am. Chem. Soc. 125 (2003) 8614–8624.
[11] United States Geological Survey, in: U.S. D.o.t. Interior (Ed.), Mineral Commodity Summaries 2011, 2001, p. 198.
[12] P.H. Kuck, in: U.S. D.o.t. Interior (Ed.), Nickel – 2009 [Advanced Release], 2011.
[13] P.J. Loferski, in: U.S. D.o.t. Interior (Ed.), Platinum-Group Metals – 2009 [Advance Release], 2011.
[14] B. Butschke, H. Schwarz, Organometallics 30 (2011) 1588–1598.
[15] G. Takahashi, E. Shirakawa, T. Tsuchimoto, Y. Kawakami, Adv. Synth. Catal. 348 (2006) 837–840.
[16] H. Ma, S. Chattopadhyay, J.L. Petersen, M.P. Jensen, Inorg. Chem. 47 (2008) 7966–7968.
[17] T.R. Cundari, T.V. Grimes, T.B. Gunnoe, J. Am. Chem. Soc. 129 (2007) 13172–13182.
[18] T.R. Cundari, J.O.C. Jimenez-Halla, G.R. Morello, S. Vaddadi, J. Am. Chem. Soc. 130 (2008) 13051–13058.
[19] M.J. Frisch, G.W. Trucks, H.B. Schlegel, G.E. Scuseria, M.A. Robb, J.R. Cheeseman, J.A. Montgomery, T. Vreven, K.N. Kudin, J.C. Burant, J.M. Millam, S.S. Iyengar, J. Tomasi, V. Barone, B. Mennucci, M. Cossi, G. Scalmani, N. Rega, G.A. Petersson, H. Nakatsuji, M. Hada, M. Ehara, K. Toyota, R. Fukuda, J. Hasegawa, M. Ishida, T. Nakajima, Y. Honda, O. Kitao, H. Nakai, M. Klene, X. Li, J.E. Knox, H.P. Hratchian, J.B. Cross, V. Bakken, C. Adamo, J. Jaramillo, R. Gomperts, R.E. Stratmann, O. Yazyev, A.J. Austin, R. Cammi, C. Pomelli, J.W. Ochterski, P.Y. Ayala, K. Morokuma, G.A. Voth, P. Salvador, J.J. Dannenberg, V.G. Zakrzewski, S. Dapprich, A.D. Daniels, M.C. Strain, O. Farkas, D.K. Malick, A.D. Rabuck, K. Raghavachari, J.B. Foresman, J.V. Ortiz, Q. Cui, A.G. Baboul, S. Clifford, J. Cioslowski, B.B. Stefanov, G. Liu, A. Liashenko, P. Piskorz, I. Komaromi, R.L. Martin, D.J. Fox, T. Keith, M.A. Al-Laham, C.Y. Peng, A. Nanayakkara, M. Challacombe, P.M.W. Gill, B. Johnson, W. Chen, M.W. Wong, C. Gonzalez, J.A. Pople, Gaussian 03, Revision C.02, 2003.
[20] T.R. Cundari, W.J. Stevens, J. Chem. Phys. 98 (1993) 5555–5565.
[21] C. Lee, W. Yang, R.G. Parr, Phys. Rev. B 37 (1988) 785–789.
[22] W.J. Stevens, H. Basch, M. Krauss, J. Chem. Phys. 81 (1984) 6026–6033.
[23] W.J. Stevens, M. Krauss, H. Basch, P.G. Jasien, Can. J. Chem. 70 (1992) 612–630.

[24] A.D. Becke, J. Chem. Phys. 98 (1993) 5648–5652.
[25] A.D. Becke, J. Chem. Phys. 98 (1993) 1372–1377.
[26] B. Miehlich, A. Savin, H. Stoll, P. Heinzwerner, Chem. Phys. Lett. 157 (1989) 200–206.
[27] F.H. Allen, Acta Crystallogr. B 58 (2002) 380–388.
[28] C.M. Norris, S. Reinartz, P.S. White, J.L. Templeton, Organometallics 21 (2002) 5649–5656.
[29] G.R. Morello, T.R. Cundari, T.B. Gunnoe, J. Organometallic Chem. 697 (2010) 15–22.
[30] E. Clot, O. Eisenstein, W.D. Jones, Proc. Natl. Acad. Sci. 104 (2007) 6939–6944.
[31] A.B. Kazi, H.V. Rasika Dias, S.M. Tekarli, G.R. Morello, T.R. Cundari, Organometallics 28 (2009) 1826–1831.
[32] K.F. Hirsekorn, E.B. Hulley, P.T. Wolczanski, T.R. Cundari, J. Am. Chem. Soc. 130 (2008) 1183–1196.